Journal of
Mechanics of
Materials and Structures

RESPONSE OF SUBMERGED METALLIC SANDWICH STRUCTURES TO UNDERWATER IMPULSIVE LOADS

Siddharth Avachat and Min Zhou

Volume 10, No. 1 January 2015

msp

JOURNAL OF MECHANICS OF MATERIALS AND STRUCTURES
Vol. 10, No. 1, 2015
dx.doi.org/10.2140/jomms.2015.10.17

RESPONSE OF SUBMERGED METALLIC SANDWICH STRUCTURES TO UNDERWATER IMPULSIVE LOADS

SIDDHARTH AVACHAT AND MIN ZHOU

The response of planar sandwich structures with metallic square-honeycomb cores under high-intensity water-based impulsive loading is analyzed through fully dynamic finite element simulations. The analyses concern overall structural response, damage and energy dissipation. The steel sandwich plates considered have different contact conditions with water — an air-backed configuration which simulates contact with water on only the load side and a water-backed configuration which simulates submerged conditions. The 3D finite element simulations account for the effects of fluid-structure interactions and the ductile failure of the sandwich structure material. Results show that the primary deformation mode is core-wall buckling in light-core structures and shear-rupture in face-sheets and core-webs in heavy-core structures. On a unit weight basis, sandwich structures with heavy cores perform poorly while those with light cores exhibit superior blast-resistance in terms of back-face deflection and total energy absorbed. Significant differences between the responses of air-backed and water-backed structures are observed. An analysis is carried out to develop structure-loading-performance relations to facilitate the design of structures tailored for specific loading conditions.

1. Introduction

Marine structures are designed to operate in hostile environments consisting of corrosive seawater, hot and cold temperature extremes, transient dynamic loads from hull-slamming and complex three-dimensional hydrostatic loads. Additionally, naval structures are required to withstand impact and blast loads resulting from surface and underwater explosions. The dynamic response of structures under such conditions is complicated because of many factors, including rate effects, complex failure modes, the superposition of dynamic and static pressures, load triaxiality and varying impulsive load intensities.

In recent years, sandwich structures have become a central structural component of many naval vessels which require blast protection. This emerging trend necessitates research that accounts for constituent material behavior, structural hierarchy, topological characteristics and complex loading involving fluid-structure interactions (FSI). Experiments focusing on different core topologies and specimen sizes have been carried out by Espinosa et al. [2006] and McShane et al. [2008] using gas gun-based impact loading to generate underwater pressure impulses, and by Dharmasena et al. [2008] using explosive sheets to generate planar pressure impulses. Constitutive relations have been developed for sandwich structures, accounting for the crush behavior of cores and plasticity in constituents [Deshpande and Fleck 2005; Xue and Hutchinson 2004b]. It has been demonstrated that finite element analyses are capable of accurately quantifying the dynamic response of metallic sandwich structures and tracking deformation mechanisms

Keywords: steel sandwich structures, fluid-structure interactions, numerical simulation, energy dissipation, damage.

such as face-stretching, core-buckling and rupture [Côté et al. 2009; Dharmasena et al. 2010; Hutchinson and Xue 2005; Liang et al. 2005; Radford et al. 2006; McShane et al. 2006; Rathbun et al. 2006; Spuskanyuk and McMeeking 2007; Vaziri and Xue 2007; Vaziri et al. 2007; Wadley et al. 2013; Wei et al. 2008; Xue and Hutchinson 2004a; Zok et al. 2005]. The major findings from these studies include:

(1) Metallic sandwich structures outperform monolithic plates when deformation is dominated by bending. In the stretching regime, monolithic plates show higher plastic dissipation than sandwich plates.

(2) The overall deflection experienced by sandwich plates is significantly less than that experienced by monolithic plates of equivalent mass. The forces and impulses transmitted by sandwich structures are also lower than those by monolithic structures.

(3) Core design greatly influences the dynamic response of sandwich structures. The dynamic strength of the core is an important factor in overall structural response. Stiff cores perform poorly while light cores lead to more efficient blast mitigation.

(4) Homogenized continuum core models cannot accurately capture the various damage modes associated with prismatic sandwich structures. Rupture and core buckling can only be evaluated using detailed finite element simulations with explicit account of structures.

(5) FSI effects need to be considered to accurately characterize impulsive loads and can be exploited to improve blast mitigation in marine structures. Sandwich structures subjected to exponentially decaying pressure pulses outperform those subjected to instantaneous loads.

While these findings provide significant insight, the relationship between performance in terms of failure resistance and energy dissipation and design parameters of sandwich structures has not been well quantified. Structural design of ships and submersibles is a complex undertaking, because the deformations experienced by naval vessels are a result of the combined effects of multiple loads acting simultaneously. Geometric and material nonlinearities create complicated loading conditions and often cause unpredictable failure through buckling and shear cracking. The effective design of naval structures requires an understanding of the failure characteristics of advanced materials and structures, and the capability to predict and determine their performance characteristics.

The objective of this analysis is to identify deformation mechanisms leading to ultimate failure and develop quantitative material-property-performance relations to aid the development of blast-resistant metallic sandwich structures. Simulations are carried out for a range of impulsive load intensities and two distinct loading configurations: (1) an air-backed configuration, with the structure in contact with water on the impulse side, and (2) a water-backed configuration, with the structure in contact with water on the impulse side as well as the backside. The structure-performance relations presented here focus on optimal core, front-face and back-face masses as fractions of total structural mass. The analysis yields the optimal values of these attributes, which in turn determine the core mass fraction $\overline{M}_{\mathrm{C}}$, the front face mass fraction $\overline{M}_{\mathrm{FF}}$, and back face mass fraction $\overline{M}_{\mathrm{BF}}$. The results are presented in normalized forms to gain insight into underlying trends that can be used to design more blast-resistant structures. The constitutive and damage behavior of steel is characterized by the Johnson–Cook model [1985], and the dynamic response of water is characterized by the Mie–Grüneisen equation of state. The insight gained here provides guidelines for the design of structures for which response to water-based impulsive loading is an important consideration. In order to facilitate comparison of dynamic response, all structures are

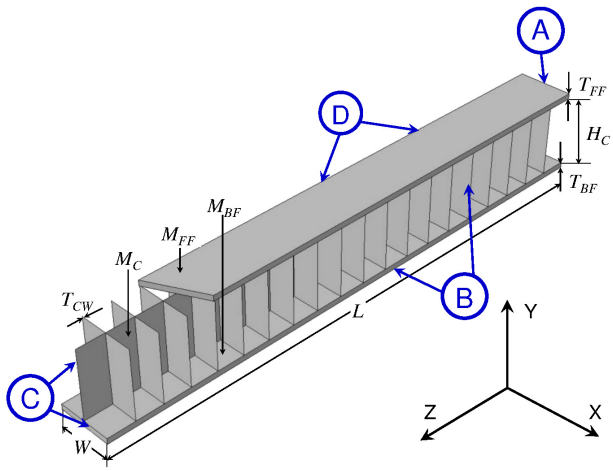

Figure 1. Schematic illustration of a sandwich beam with square honeycomb core.

designed to have the same total areal mass of $\sim 100\,\mathrm{kg/m^2}$. This necessitates a balance in core, front face and back face masses to maintain a constant areal mass. The structures are subjected to five loading intensities, each simulating different standoff distances of an underwater explosive source from the ship hull. The design space consists of three major aspects: (1) performance parameters (deflection, energy dissipation and impulse transmission), (2) structural attributes (core mass, front-face mass and back-face mass), and (3) loading intensity. These parameters and their effects are intimately interrelated. The structural composition of the sandwich structure is systematically varied over a wide range of structural attributes with simultaneous variations in loading rates to delineate the effects of each parameter on dynamic performance and blast resistance. This approach enables the contributions of different deformation mechanisms (front-face stretching and rupture, core-wall buckling, core crushing and back-face stretching) to be tracked and quantified. Additionally, this approach captures the interaction and coupling of the different design parameters at the structural level. The analyses also focus on the correlation between mass fractions of each structural component (front face, core and back face), deflection, energy dissipation and impulse transmission. The results of parametric studies are presented in a format wherein the response variables are functions of the loading (impulse magnitude) and structural attributes (mass fractions of each structural component).

2. Framework of analysis

2.1. ***Structure specifications.*** The square honeycomb sandwich plates considered are made of AISI 304 steel. Figure 1 shows the sandwich structure consisting of a core with periodic square-honeycomb unit-cells and face sheets. The core-height H_C is 100 mm and the length L of the beam is 1000 mm. The core-height to beam-length ratio H_C/L is 0.1. For the sandwich structure, face A is fixed (zero displacement and rotations in all directions), faces B and D have boundary conditions that forbid displacement in the x-direction, and face C has symmetry boundary conditions with the plane of symmetry normal to the z-direction. The boundary conditions and specified dimensions are sufficient to ensure beam bending

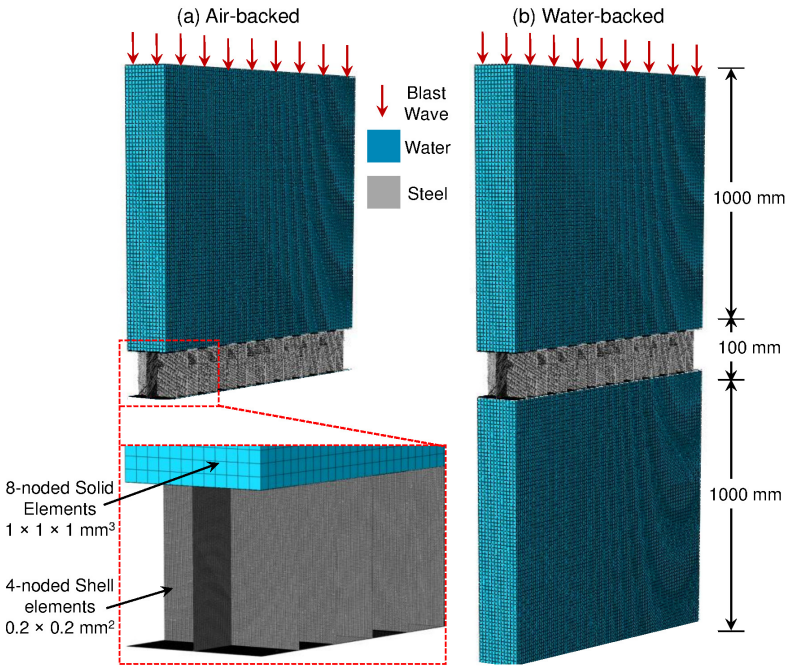

Figure 2. Sandwich structures with edge-supported boundaries and air-backed and water-backed loading configurations.

behavior [Wicks and Hutchinson 2001; Zok et al. 2003]. Figure 2 shows the air-backed and water-backed loading configurations with the direction of impulsive loading. The width W of the sandwich beam is 100 mm. The areal mass of the sandwich structure is calculated as

$$M_{\text{Total}} = M_{\text{FF}} + M_{\text{BF}} + M_{\text{C}} = \frac{\rho}{A}(T_{\text{FF}} \cdot A \cdot W + T_{\text{BF}} \cdot A \cdot W + N_{\text{CW}} \cdot T_{\text{CW}} \cdot H_{\text{C}} \cdot L), \tag{1}$$

where M_{FF} is the areal mass of the front face, M_{BF} is the areal mass of the back face, M_{C} is the areal mass of the core, ρ_{Steel} is the density of steel, N_{CW} is the number of unit cells in the square honeycomb, H_{C} is the height of the core, T_{CW} is the core wall thickness, A is the area under loading, W is the width of the structure, and L is the length of the structure. The total areal mass of the plate, M_{Total}, is kept constant at 100 kg/m^2. The normalized core mass is

$$\overline{M}_{\text{C}} = \frac{M_{\text{C}}}{M_{\text{Total}}}, \tag{2}$$

the normalized front face mass is

$$\overline{M}_{\text{FF}} = \frac{M_{\text{FF}}}{M_{\text{Total}}}, \tag{3}$$

and the normalized back face mass is

$$\overline{M}_{\text{BF}} = \frac{M_{\text{BF}}}{M_{\text{Total}}}. \tag{4}$$

Specimen number	Front face thickness T_{FF} (mm)	Front face mass M_{FF} (kg/m^2)	Core wall thickness T_{CW} (mm)	Core areal mass M_C (kg/m^2)	Back face thickness T_{BF} (mm)	Back face mass M_{BF} (kg/m^2)	Areal mass M_{Total} (kg/m^2)
1	1.0	8	3.62	84	1.0	8	100
2	2.0	16	2.93	68	2.0	16	100
3	3.0	24	2.24	52	3.0	24	100
4	4.0	32	1.55	36	4.0	32	100
5	5.0	40	0.86	20	5.0	40	100
6	5.6	45	0.43	10	5.6	45	100

Table 1. Structural configurations analyzed for the optimization of core mass.

Specimen number	Front face thickness T_{FF} (mm)	Front face mass M_{FF} (kg/m^2)	Core wall thickness T_{CW} (mm)	Core areal mass M_C (kg/m^2)	Back face thickness T_{BF} (mm)	Back face mass M_{BF} (kg/m^2)	Areal mass M_{Total} (kg/m^2)
1	0.5	4	0.86	20	9.5	76	100
2	1.0	8	0.86	20	9.0	72	100
3	2.0	16	0.86	20	8.0	64	100
4	3.0	24	0.86	20	7.0	56	100
5	4.0	32	0.86	20	6.0	48	100
6	5.0	40	0.86	20	5.0	40	100

Table 2. Structural configurations analyzed for the optimization of face mass.

To evaluate the role of core strength in the deformation, $\overline{M}_C$ is varied from 0.10 to 0.84 by changing the core wall thicknesses. To keep the total mass constant, the changes in core mass are compensated by variations in the masses of the face sheets. Table 1 shows the structural parameters used in the core mass optimization. Structures with $0.10 < \overline{M}_C < 0.5$ are called *light core* structures, while those with $0.5 < \overline{M}_C < 1$ are called *heavy core* structures. For the optimized core mass fraction, the front and back face thicknesses are varied to evaluate the role of face strength in dynamic deformation. For this, the normalized front face mass $\overline{M}_{FF}$ is varied from 0.04 to 0.4 and the corresponding normalized back face mass $\overline{M}_{BF}$ is varied from 0.86 to 0.50. Table 2 shows the structural parameters used for the optimization of front and back face masses. These structures are subjected to a range of impulsive loads in both air-backed and water-backed conditions.

2.2. ***Impulsive loading.*** A number of approaches have been used to simulate the interactions of blast waves with structures, both in air and underwater. One approach is to simulate the fluid with Eulerian meshes and the solid structure with Lagrangian meshes. The behavior of the fluid in the Eulerian domain can be modeled using an equation of state. This technique is termed the "arbitrary Lagrangian–Eulerian" method and is often used to simulate the fluid structure interactions when large mesh distortions in the

fluid domain are a major concern [Battley and Allen 2012; Latourte et al. 2012]. The second approach is to prescribe an exponentially decaying pressure on one face of the structure [Dharmasena et al. 2011; Wadley et al. 2013] to account for the effect of the fluid. The incident impulse can be calculated using [ConWep 2005], a blast simulation code developed by the U.S. Army Corps of Engineers, which allows the impulse to be determined for given explosive charge and standoff distance between the charge and the target. A third approach is to simulate both the fluid and the structure with Lagrangian elements [Mori et al. 2007]. An appropriate equation of state is chosen to describe the response of the fluid. In this study, the third approach with a Lagrangian formulation for both the fluid and the structure is employed.

According to Taylor's analysis [1963] of one-dimensional blast waves for a plane wave impinging on a free-standing plate, the pressure in the fluid at a fixed position follows the relation

$$p(t) = p_0 \exp(-t/t_0), \tag{5}$$

where p_0 is the peak pressure, t is time and t_0 is the reference decay time. The area under this curve is the impulse I imparted by the wave:

$$I = \int_0^{t_0} p(t)\, dt. \tag{6}$$

A nondimensionalized impulse $\bar{I}$ can be expressed as

$$\bar{I} = \frac{I}{\rho_w c_w \sqrt{A}}, \tag{7}$$

where ρ_w is the density of water, c_w is the speed of sound in water and A is the area of loading. Impulsive waves due to underwater blasts have a characteristic decay time on the order of $\sim 10^{-4}$ seconds [Cole 1947; Kambouchev et al. 2007; Taylor 1963]. The numerical modeling simulates the effects of different standoff distances of an explosive source. For an underwater explosion, the peak pressure (in MPa) scales as

$$p_0 = 52.4\left(\frac{M^{1/3}}{r}\right)^{1.13}, \tag{8}$$

where M is the mass of trinitrotoluene (TNT) in kilograms and r is the standoff distance in meters [Cole 1947; Kambouchev et al. 2007; Taylor 1963].

Figure 3 shows the pressure histories of impulsive loads considered in the finite element simulations. The reference decay time (t_0) is $\sim 250\,\mu$s. The rise time of the pressure pulses is on the order of 25 μs and the time for the pressure to decrease to negligible levels is on the order of 800 μs. The impulsive loads considered in this set of calculations have peak pressures of 450, 350, 250, 150 and 50 MPa, which approximately correspond to 100 kg of TNT exploding at distances of 0.7, 0.9, 1.15, 1.8 and 4.8 meters, respectively. The impulsive load is planar, the sandwich structure is in the form of a beam and a single repeating unit cell along the x-direction (shown in Figure 2) is analyzed.

A number of load conditions and service environments exist for sandwich structures in large naval structures, such as ships or submarines. For example, ship hulls and superstructures are in touch with water on the outer side (impulse side) and air or machinery on the inner side. On the other hand, keels, rudders, propeller blades and underwater pipelines consist of water on both the impulse side and the protected side. For the purpose of the current study, the former is called the air-backed configuration (Figure 2(a)) and the latter is called the water-backed configuration (Figure 2(b)). In both air-backed

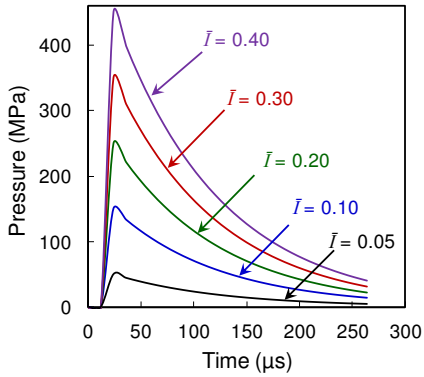

Figure 3. Pressure histories of incident impulsive waves incident on sandwich structures.

and water-backed configurations, the length of the impulse-side water column is 1000 mm. In the water-backed configuration, the length of the back-side water column is also 1000 mm. The length is sufficient to ensure that reflected waves do not interfere with deformations in the structure prior to 1000 μs.

3. Numerical calculations

The faces and core webs are meshed with 4-noded shell elements for finite strains to capture buckling and rupture. In the initial steps, nodes are adjusted with strain-free displacements to remove any surface interpenetration. A penalty contact algorithm is used at all interfaces to strongly discourage interpenetration by applying penalty forces. Specifically, an interface "spring" is inserted between the slave and master nodes and penalty forces at each instance of interpenetration are calculated by multiplying the spring stiffness with the penetration distance. The penalty contact framework seeks to resolve contact penetrations that exist at the beginning of each time increment. This ensures that surface interpenetrations are negligible and do not affect the deformation mechanisms in the different components of the sandwich structure. The response of the structures is partly quantified using the deflection at the center of the back face and the energy dissipated through plastic deformation and damage due to crack initiation and growth. These quantities depend on structural parameters, loading configuration and impulse magnitude. Damage in the forms of core crushing, core-web cracking and face-sheet rupture is tracked. The calculations are conducted using the ABAQUS/Explicit finite-element package [Hibbit et al. 2009].

3.1. ***Constitutive and damage models for steel.*** The sandwich plates studied here are made of AISI 304 steel, which has high yield strength, high strain hardening and high ductility. The Johnson–Cook model [Johnson and Cook 1985], which accounts for strain-hardening, thermal softening, and strain rate dependence is used to describe the material's response. Specifically,

$$\bar{\sigma}(\bar{\epsilon}^{\mathrm{pl}}, \dot{\epsilon}^{\mathrm{pl}}, \theta) = (A + B(\bar{\epsilon}^{\mathrm{pl}})^n)\left(1 + C \ln \frac{\dot{\epsilon}^{\mathrm{pl}}}{\dot{\epsilon}_0}\right)(1 - (\hat{\theta})^m), \tag{9}$$

where $\bar{\sigma}$ is the Mises equivalent stress, $\bar{\epsilon}^{\mathrm{pl}}$ is the equivalent plastic strain, $\dot{\epsilon}^{\mathrm{pl}}$ is the equivalent plastic strain rate, and A, B, C, m and n are material parameters measured at or below the transition temperature

$\theta_{\text{transition}}$, $\dot{\epsilon}_0$ is a reference strain rate, and $\hat{\theta}$ is the nondimensional temperature, defined as

$$\hat{\theta} \equiv \begin{cases} 0 & \text{for } \theta < \theta_{\text{transition}}, \\ (\theta - \theta_{\text{transition}})/(\theta_{\text{melt}} - \theta_{\text{transition}}) & \text{for } \theta_{\text{transition}} \le \theta \le \theta_{\text{melt}}, \\ 1 & \text{for } \theta > \theta_{\text{melt}}. \end{cases} \tag{10}$$

In these expressions, θ is the current temperature, θ_{melt} is the melting temperature and $\theta_{\text{transition}}$ is the transition temperature below which the yield stress is independent of the temperature. When the temperature exceeds the melting temperature, the material behaves like a fluid and has no shear resistance. The use of the Johnson–Cook constitutive model partly reflects the nature of the deformations analyzed and partly reflects the fact that extensive experimental data is available and has been used to calibrate this model for the conditions analyzed. Indeed, there are more "sophisticated" models than the Johnson–Cook model. These models use different parameters or internal state variables to deal with issues such as complicated loading paths, varying stress triaxiality, and deformation mechanisms. However, the key aspects of the loading conditions analyzed in this paper are dynamic, rate-dependent, monotonic (no unloading considered), and approximately proportional. Under such conditions, the constitutive response of the steels considered here can be well-characterized as dependent on strain, strain rate and temperature. Models using relations between stress and these quantities are effectively similar or equivalent, as long as enough parameters exist to allow a good fit to experimental data. For the conditions stated above, many more sophisticated models using, say, certain internal state variables essentially simplify to relations involving stress, strain, strain rate and temperature as independent variables.

The failure model is based on the value of equivalent plastic strain. The damage parameter ω is defined as

$$\omega = \sum \left(\frac{\Delta \bar{\epsilon}^{\text{pl}}}{\bar{\epsilon}_f^{\text{pl}}} \right), \tag{11}$$

where $\Delta \bar{\epsilon}^{\text{pl}}$ is an increment of the equivalent plastic strain, $\bar{\epsilon}_f^{\text{pl}}$ is the strain at failure, and the summation is performed over all increments up to the current state in the analysis. The strain at failure is assumed to be dependent on strain rate and temperature such that

$$3\bar{\epsilon}_f^{\text{pl}} = \left(D_1 + D_2 \exp(-D_3 p/\bar{\sigma})\right)\left(1 + D_4 \ln \frac{\dot{\bar{\epsilon}}^{\text{pl}}}{\dot{\epsilon}_0}\right)(1 + D_5 \hat{\theta}), \tag{12}$$

where D_1, D_2, D_3, D_4, and D_5 are experimentally determined damage parameters, $p = -\sigma_{ii}/3$ is the hydrostatic pressure. The values for the parameters are obtained from [Johnson and Cook 1985] and [Nahshon et al. 2007] and are shown in Table 3.

3.2. ***Mie–Grüneisen equation of state for water.*** The response of water is modeled with the Mie–Grüneisen equation of state of the linear Hugoniot form:

$$p = \frac{\rho_0 c_0^2 \eta}{(1 - s\eta)^2}\left(1 - \frac{\Gamma_0 \eta}{2}\right) + \Gamma_0 \rho_0 E_m, \tag{13}$$

where p is pressure, c_0 is the speed of sound in bulk, ρ_0 is the initial density, η is the volumetric compressive strain, E_m is internal energy per unit mass, Γ_0 is Grüneisen's gamma at reference state,

Density of steel (ρ_{Steel})	7800 kg/m^3
Young's modulus (E)	193 GPa
Poisson's ratio (ν)	0.3
Melting temperature (θ_{melt})	1800 °C
Reference temperature (θ)	25 °C
Density of water (ρ_{Water})	1000 kg/m^3
Speed of sound in water (c_0)	1500 m/s
Grüneisen's gamma for water (Γ_0)	0.1

A	310 MPa
B	1000 MPa
n	0.65
C	0.034
m	1.05
D_1	0.25
D_2	4.38
D_3	2.68
D_4	0.002
D_5	0.61

Table 3. Parameters for constitutive and damage models.

$s = dU_s/dU_p$ is the linear Hugoniot slope coefficient, U_s is the shock wave velocity and U_p is particle velocity, which is related to U_s through

$$U_s = c_0 + sU_p. \tag{14}$$

4. Results and discussion

4.1. ***Parametric analysis and comparison with experiments.*** A parametric study is carried out, focusing on the effects of (i) loading intensity, (ii) changes in core and face properties, and (iii) air-backed and water-backed configurations on dynamic response. The objective is to quantify the relationship between the response of the structures, loading intensities, material properties and structural attributes. The loading configuration is shown in Figure 2, and the sandwich plate studied is shown in Figure 1. Although five different impulsive load levels are considered, for brevity we focus on the deformation histories for the load intensity of $\bar{I} = 0.2$ in the following section.

The results of the finite element simulations are compared with experimental results in the literature. Figure 4 shows the deformed configurations of a light-core sandwich structure ($\overline{M}_{\text{C}} = 0.197$) with a prismatic core subjected to impulsive loading with $\bar{I} = 0.2$. Results are compared to simulations for the sandwich structure with $\overline{M}_{\text{C}} = 0.2$. Comparing the simulations with experimental measurements shows that the simulations capture a majority of the details of the deformation mechanisms quite realistically. These include core wall buckling, core shearing and stress concentrations near the clamped edges. The debonding due to core wall buckling is also represented in the simulations. In both the simulations and experiments, the face sheets undergo yielding but do not experience fracture and separation from the supports. The front face experiences tensile stretching while the back face is relatively undamaged. The experimental results are obtained by Dharmasena et al. [2008]. In experiments, different masses of TNT at a fixed standoff distance of 10 cm are used to create impulsive loads. In experiments, the core has a wall thickness of 0.76 mm and the face sheet thickness is 5 mm, such that $\overline{M}_{\text{C}} = 0.197$, compared to $\overline{M}_{\text{C}} = 0.2$ in simulations. The comparison between experiments and simulations shows good agreement in terms of damage mechanisms and structural deformation. Overall, experimentally observed deformation mechanisms are reasonably replicated in the simulations.

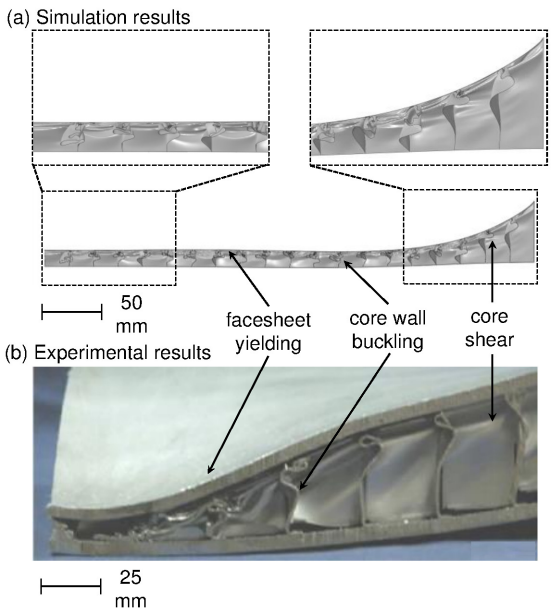

Figure 4. Comparison of computational and experimental deformation modes in a sandwich panel subjected to an impulsive load. Experimental results are obtained from [Dharmasena et al. 2008]. The sandwich core consists of a square honeycomb topology with $\overline{M}_{\mathrm{C}} = 0.197$ for experiments and $\overline{M}_{\mathrm{C}} = 0.20$ for the simulations.

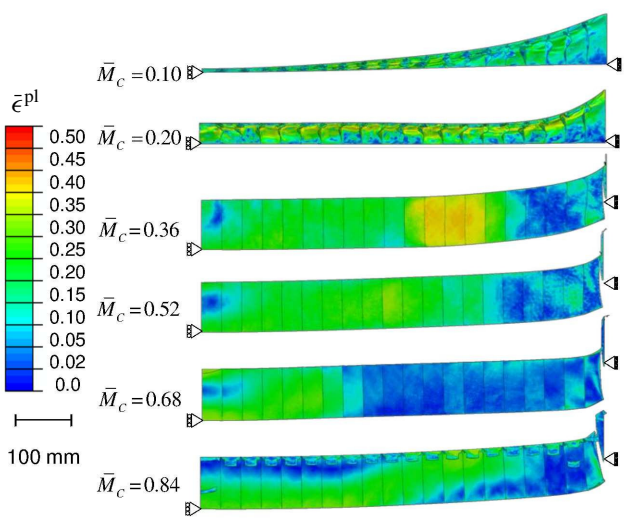

Figure 5. Distributions of equivalent plastic strain for *air-backed* structures with different $\overline{M}_{\mathrm{C}}$ values and an impulse of $\bar{I} = 0.2$. The overall deflection increases as $\overline{M}_{\mathrm{C}}$ increases. The structure with $\overline{M}_{\mathrm{C}} = 0.10$ exhibits the most deformation through core-wall buckling. Structures with $\overline{M}_{\mathrm{C}} > 0.2$ experience core-stretching and shear rupture. The corresponding front- and back-face masses are given in Table 1.

4.2. ***Deformation mechanisms in air-backed structures.*** Figure 5 shows the distributions of equivalent plastic strain for structures with different values of $\overline{M}_C$ for $\bar{I} = 0.2$ at $t = 1000\,\mu$s. This figure reveals the role of core stiffness. For $\overline{M}_C = 0.10$, the lightest core, the response is dominated by core wall buckling and front face stretching, with no rupture. For $\overline{M}_C = 0.20$, core wall buckling and stretching occur simultaneously, with the onset of rupture delayed due to higher core compliance. Structures with $\overline{M}_C = 0.10$ and $\overline{M}_C = 0.20$ are the only cases showing no rupture up to $t = 1000\,\mu$s. As $\overline{M}_C$ increases beyond 0.20, the failure mode changes from tensile stretching and core wall buckling to shear-dominated rupture. The configurations with $\overline{M}_C = 0.36$, 0.54 and 0.68 exhibit fracture and catastrophic failure due to localized deformation. Clearly, equitable distribution of mass between the front face, core and back face does not provide optimal blast mitigation. For $\overline{M}_C = 0.84$, the case with the heaviest core considered, the core-face junctions are locations of severe stress concentration and failure.

For all cases considered, two competing deformation mechanisms — core compression and overall beam bending — are observed. Light-core structures undergo severe core compression without significant bending. Light cores allow the structure to attain a common velocity after $\sim 600\,\mu$s for $\overline{M}_C = 0.20$ and $\sim 800\,\mu$s for $\overline{M}_C = 0.10$; these times are five times longer than those for heavy core structures. Structures with $0.04 < \overline{M}_C \leq 0.20$ do not undergo shear rupture. On the other hand, heavy cores minimize core crushing and lead to significant bending deformation, ultimately causing rupture. The structure acquires a common velocity after $\sim 250\,\mu$s for $\overline{M}_C = 0.84$ and $\sim 350\,\mu$s for $\overline{M}_C = 0.52$.

4.3. ***Deformation mechanisms in water-backed structures.*** A comparison of the results for air-backed and water-backed structures reveals significant differences in deformation and failure mechanisms. The presence of a dense medium (water) on both sides of the structure prevents large scale bending and leads to higher internal energy dissipation. The absence of bending leads to greater front face-core interactions and core compression but creates a cushioning effect for the back face. To quantify the differences between these two configurations, a comparative study is carried out.

Figure 6 shows the distributions of equivalent plastic strain for water-backed structures with different $\overline{M}_C$ values and $\bar{I} = 0.2$ at $t = 1000\,\mu$s. For $\overline{M}_C = 0.10$, the core has very low resistance to wall buckling and, consequently, core-crushing initiates upon the onset of loading. When the core collapses, the front face strikes the back face and the stress wave passes through the back face into the surrounding water. For $\overline{M}_C = 0.20$, structural deflection as well as core wall buckling are observed. For $\overline{M}_C = 0.34$, core crushing is negligible and core stretching is more intense than those for structures with $\overline{M}_C = 0.20$ and $\overline{M}_C = 0.10$. Due to the presence of the back-side water, the back-face displacement is very small and no rupture is observed near the support. However, for all structural configurations with $\overline{M}_C > 0.36$, rupture initiates near the support in the front face, core and back face. As core mass increases, the stress concentration near the support becomes more severe and causes fracture and separation. Clearly, heavy cores are detrimental to blast resistance in both air-backed and water-backed structures.

Although heavy core designs are undesirable under both air-backed and water-backed conditions, water-backed structures with heavy cores can sustain larger impulses because a large fraction of the incident impulse is transmitted through the back face into the surrounding water and structural deflection is constrained. A major distinction between air-backed and water-backed structures is that in air-backed structures, the impulse is transmitted to the supports while in water-backed structures, the impulse is transmitted to the surrounding water.

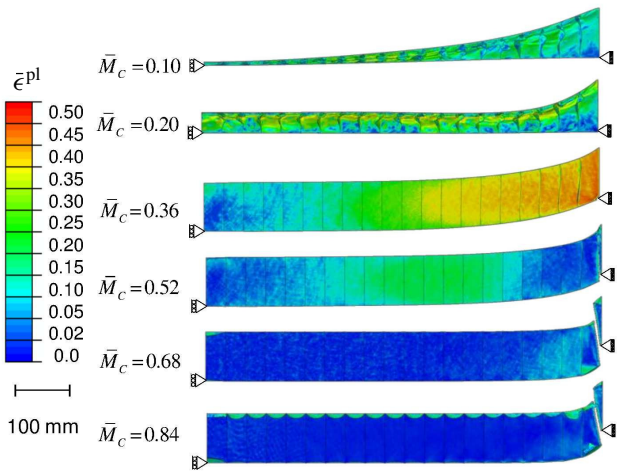

Figure 6. Distributions of equivalent plastic strain for *water-backed* structures with different $\overline{M}_C$ values and an impulse of $\bar{I} = 0.2$. The overall deflection is essentially the same for all values of $\overline{M}_C$. The structure with $\overline{M}_C = 0.10$ exhibits the most deformation through core-wall buckling. Structures with $\overline{M}_C > 0.36$ show shear rupture. The corresponding front- and back-face masses are given in Table 1.

4.4. ***Deflection.*** To evaluate and compare the responses, the deflections at the midpoints of the back faces at 600 μs for six different sandwich structures and five different impulse magnitudes are measured and compared. The deflections are normalized by the length of the structure span. Figure 7 shows the normalized deflection Δ/L in the front face and back face as a function of normalized core mass $\overline{M}_C$ and normalized impulse $\bar{I}$ for air-backed and water-backed structures. As discussed previously, structures with low $\overline{M}_C$ exhibit higher core compression and, as $\overline{M}_C$ increases, core compression decreases. For $\overline{M}_C \leq 0.20$, the front face deflects much more than the back face due to high core compression. Conversely, for $\overline{M}_C > 0.20$, the front and back faces undergo essentially the same deflection due to negligible core compression. For $\bar{I} > 0.2$, the cases with $\overline{M}_C > 0.20$ undergo rupture near the support, leading to higher overall deflections, while the cases with $\overline{M}_C \leq 0.20$ experience core crushing but no rupture. This is reflected in the large jump in the deflection between $\overline{M}_C = 0.20$ and $\overline{M}_C = 0.36$ for $\bar{I} = 0.3$ and $\bar{I} = 0.4$. At high impulse magnitudes, $\overline{M}_C \leq 0.20$ provides superior blast resistance. The structure-performance relations useful for sandwich structure design have been presented using the form

$$z = A \cdot x^m \cdot y^n, \tag{15}$$

where z is a performance parameter (Δ/L, $\overline{U}$ or $\bar{I}_T$), x is a structural attribute ($\overline{M}_C$, $\overline{M}_{FF}$ or $\overline{M}_{BF}$), y is the load intensity and A, m and n are constants specific to each load configuration (air-backed, water-backed). More details about the structure-performance relations are provided in Section 4.9. The relationship between deflection in air-backed structures $(\Delta/L)_{AB}$, and incident impulse ($\bar{I}$) and normalized core mass ($\overline{M}_C$) can be quantified by

$$(\Delta/L)_{AB} = 1.58 \cdot (\overline{M}_C)^{0.24} \cdot \bar{I}^{0.86}. \tag{16}$$

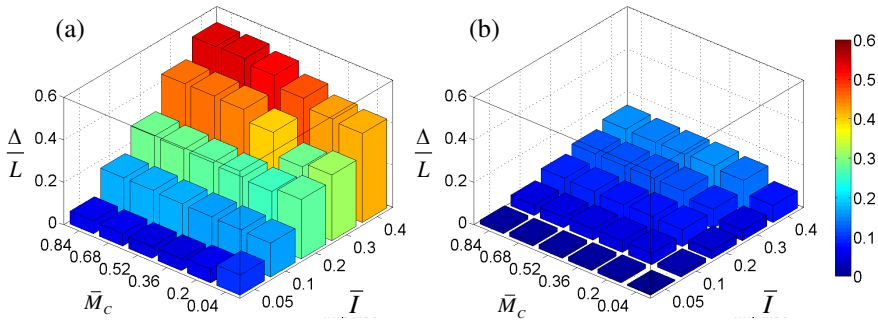

Figure 7. Normalized deflection Δ/L as a function of normalized core-mass $\overline{M}_{\mathrm{C}}$ and normalized impulse $\bar{I}$ for (a) air-backed and (b) water-backed structures. The corresponding front- and back-face masses are given in Table 1.

Figure 7(b) shows the deflection for water-backed structures as a function of normalized core mass $\overline{M}_{\mathrm{C}}$ and normalized impulse $\bar{I}$. Due to the presence of water on both sides of the structure, deflection is limited. As the load intensity increases from $\bar{I} = 0.05$ to $\bar{I} = 0.4$, the increase in the overall deflection is relatively minor. Compared with the defection in air-backed structures, the deflection for water-backed cases is $\sim 70\%$ lower for $\overline{M}_{\mathrm{C}} \leq 0.20$ and $\sim 40\%$ lower for $\overline{M}_{\mathrm{C}} > 0.20$ at high load magnitudes. For both air-backed and water-backed structures, the minimum value of Δ/L is seen for $\overline{M}_{\mathrm{C}} \leq 0.20$. Cores with wall buckling as the primary deformation mechanism show superior blast resistance than cores with core stretching as the primary deformation mechanism. The lower deflection values in water-backed cases have a significant influence on energy absorption. The relationship between deflection in water-backed structures $(\Delta/L)_{\mathrm{WB}}$, and incident impulse $(\bar{I})$ and normalized core mass $(\overline{M}_{\mathrm{C}})$ can be quantified by

$$(\Delta/L)_{\mathrm{WB}} = 0.43 \cdot (\overline{M}_{\mathrm{C}})^{0.22} \cdot \bar{I}^{0.85}. \tag{17}$$

4.5. ***Energy absorption.*** When an impulsive wave interacts with a structure, a number of energy dissipation mechanisms are activated. A significant fraction of the incident energy is dissipated through plastic deformation. The primary mechanisms of plastic dissipation include tensile stretching in the front face, core walls and back face, and core-wall buckling. A nondimensionalized dissipation measure is

$$\bar{U} = \frac{U}{L \cdot W \cdot \sigma_y \cdot (M_{\mathrm{Total}}/\rho_{\mathrm{Steel}})}, \tag{18}$$

where U is the total dissipation through plasticity; L, W and M_{Total} are the length, width and total areal mass of the sandwich structure, respectively; and σ_y and ρ_{Steel} are the yield stress and density of steel, respectively.

It is important to understand how the dissipation is distributed in the structures. In particular, the rate of dissipation as a function of time in different components of a structure can highlight regions that have the most influence on the total energy dissipation. Figure 8 shows the time histories of dissipation in different parts of a structure with $\overline{M}_{\mathrm{C}} = 0.10$ under $\bar{I} = 0.2$ for air-backed and water-backed conditions. In the air-backed case, energy absorption in the core and front face occurs simultaneously and at approximately the same rate. The motion of the front face causes core compression, plastic stretching in the front face

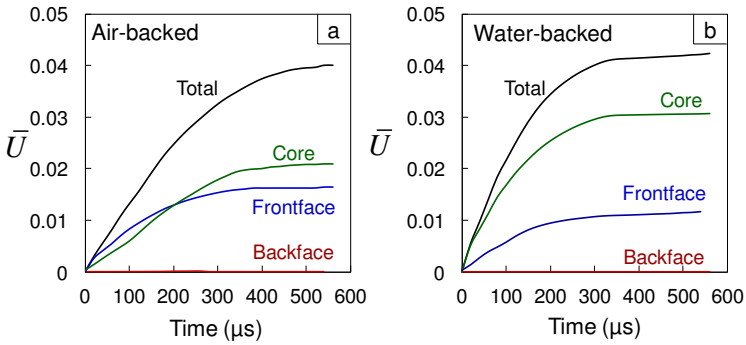

Figure 8. Plastic dissipation in (a) air-backed and (b) water-backed structures with $\overline{M}_C = 0.20$ subjected to an impulse $\bar{I} = 0.2$. The corresponding front- and back-face masses are given in Table 1.

and core-wall buckling. At $t = 200\,\mu$s, dissipation in the core surpasses that in the front face. The back face experiences negligible plastic deformation. In the water-backed structures, the low overall deflection limits the stretching of the front face and back face. Since the compressive strain in the core is much higher than that in the air-backed case, a much higher fraction of total energy absorption occurs in the core. Specifically, the core dissipates $\sim 40\%$ of the total energy in the air-backed case and $\sim 80\%$ of the total energy in the water-backed case. The time scales for the two cases are also different, with the dissipation reaching a maximum value at $\sim 500\,\mu$s in the air-backed case and at $\sim 300\,\mu$s in the water-backed case.

Figure 9 shows the normalized dissipation $\overline{U}$ in the entire structure as a function of core mass $\overline{M}_C$ and impulse $\bar{I}$ for air-backed and water-backed structures. Air-backed structures with $\overline{M}_C = 0.10$ experience low deflection and low core compression and hence absorb $\sim 20\%$ lesser energy than structures with $\overline{M}_C = 0.20$, which experience high levels of dissipation because the core webs are sufficiently thin to stretch under tensile loading induced by large deflections and sufficiently thick to prevent core-wall buckling. Structures with $\overline{M}_C > 0.20$ absorb less energy because of rupture due to localized plastic deformation and damage. Plastic dissipation ceases when the structures separate from the supports. The relationship between plastic dissipation in air-backed structures ($\overline{U}_{AB}$), and incident impulse ($\bar{I}$) and normalized core mass ($\overline{M}_C$) can be given by

$$\overline{U}_{AB} = 0.22 \cdot (\overline{M}_C)^{-0.20} \cdot \bar{I}^{1.07}. \tag{19}$$

In Figure 10, the energy absorption in water-backed structures as a function of normalized core mass $\overline{M}_C$ and impulse $\bar{I}$ follows a trend similar to that for air-backed structures, with the dissipation in the core accounting for the largest fraction of the total dissipation. The energy imparted to a sandwich structure during an underwater blast is partly converted to kinetic energy when the structure acquires velocity and deflects. In the air-backed cases, this kinetic energy is dissipated over a duration of $\sim 500\,\mu$s through face-sheet stretching, core deformation and rupture. Since water-backed structures experience low deflections and attain lower velocities, the incident energy is partially dissipated in the structure through plastic deformation and partially transmitted to the back-side water. Water-backed structures absorb $\sim 20\%$ more energy than air-backed structures under the same incident impulse, primarily due

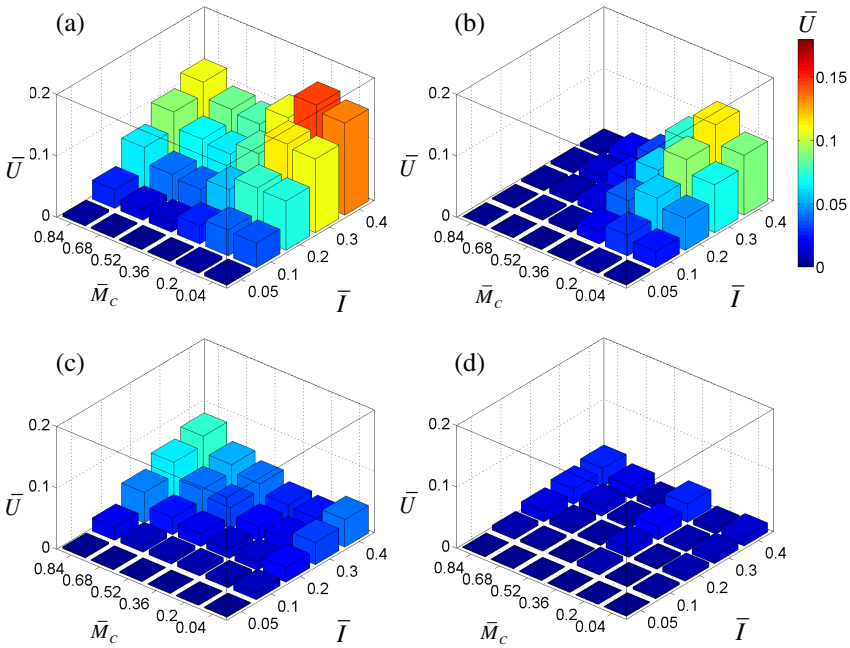

Figure 9. Normalized plastic dissipation $\bar{U}$ in air-backed structure as a function of normalized core-mass $\bar{M}_C$ and normalized impulse $\bar{I}$ for (a) entire structure, (b) core, (c) front face and (d) back face. The corresponding core, front-face and back-face masses are given in Table 1.

to more extensive core crushing. The differences in energy dissipation between air-backed and water-backed structures are negligible for $\bar{M}_C > 0.20$ under the loading conditions analyzed for the lack of plasticity. The relationship between plastic dissipation in air-backed structures ($\bar{U}_{WB}$), and incident impulse ($\bar{I}$) and normalized core mass ($\bar{M}_C$) can be stated as

$$\bar{U}_{WB} = 0.20 \cdot (\bar{M}_C)^{-0.21} \cdot \bar{I}^{0.69}. \tag{20}$$

4.6. ***Transmitted pressure in water-backed cases.*** The transmitted pressure in the back-side water is a useful parameter for quantifying the effectiveness of sandwich structures under water-backed conditions. It has significant implications for structures like cargo ships, oil tankers and pipelines. Figure 11(a) shows the histories of the downstream pressure for structures with $\bar{M}_C = 0.10$ to 0.84 under an impulse of $\bar{I} = 0.2$ which has a peak pressure of 80 MPa. For $\bar{M}_C = 0.52, 0.68$ and 0.84, the time delay for pressure transmission through the sandwich structure is $\sim 50\,\mu$s. The transmitted pressure shows an exponentially decaying profile with a peak value of 80 MPa and decay time of 600 μs. For $\bar{M}_C = 0.36$, the time delay for pressure transmission through the structure is $\sim 100\,\mu$s and the peak value and decay time of the transmitted pulse are 80 MPa and $\sim 600\,\mu$s, respectively. For $\bar{M}_C = 0.20$, the transmitted peak pressure is $\sim 30\%$ lower or approximately 55 MPa and the decay time is $\sim 400\,\mu$s. For structures with $0.20 < \bar{M}_C < 0.84$, cavitation occurs at the interface between the back face and water section. Structures with $\bar{M}_C = 0.10$ show considerably different response. Initially, cell wall buckling occurs as

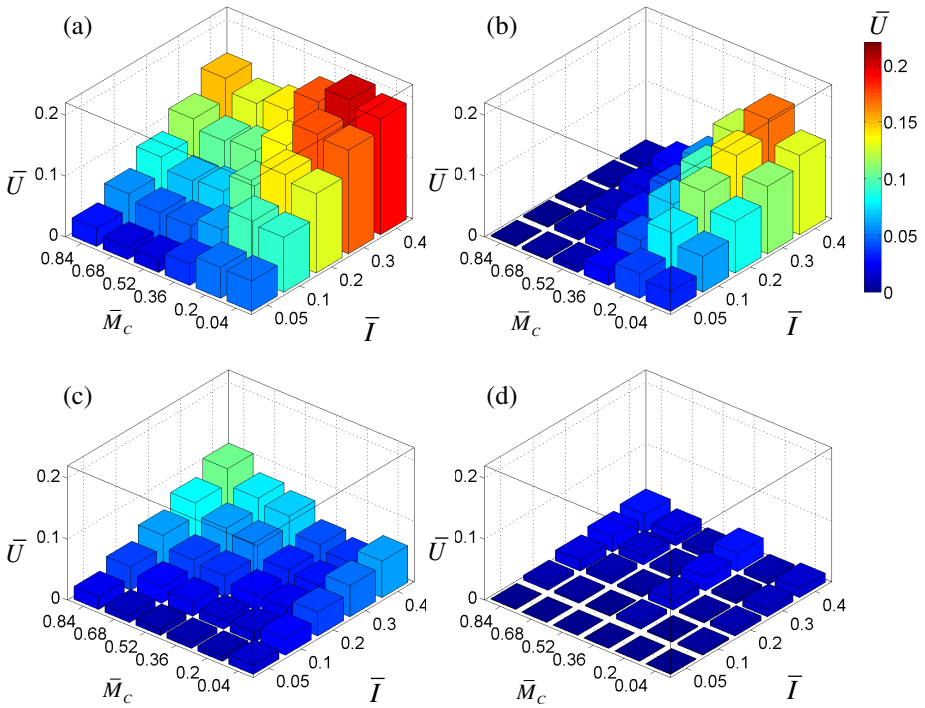

Figure 10. Normalized plastic dissipation $\bar{U}$ in water-backed structure as a function of normalized core-mass $\bar{M}_{\mathrm{C}}$ and normalized impulse $\bar{I}$ for (a) entire structure, (b) core, (c) front face and (d) back face. The corresponding core, front-face and back-face masses are given in Table 1.

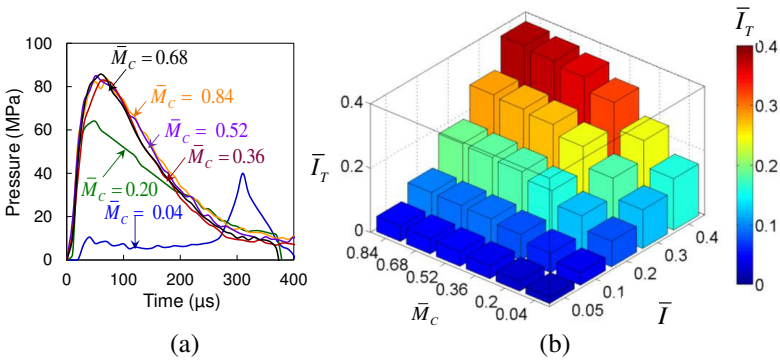

Figure 11. (a) Impulse transmission histories for $\bar{I} = 0.20$, and (b) transmitted impulse as a function of incident impulse $\bar{I}$ and normalized core mass $\bar{M}_{\mathrm{C}}$, with $\bar{M}_{\mathrm{C}} = 0.10$ to 0.84. For $\bar{M}_{\mathrm{C}} = 0.20$, there is a reduction of $\sim 60\%$ in transmitted pressure relative to the incident pressure. The corresponding front- and back-face masses are given in Table 1.

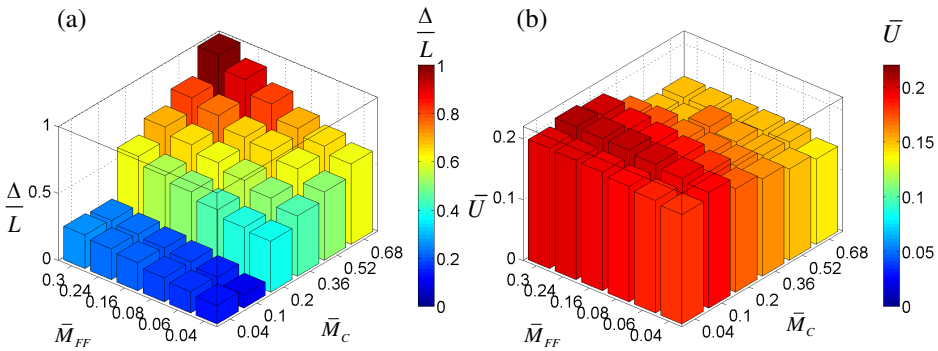

Figure 12. Normalized deflection Δ/L and plastic dissipation $\bar{U}$ in air-backed structures as functions of $\bar{M}_{\mathrm{C}}$ and $\bar{M}_{\mathrm{FF}}$. Minimum deflection is observed for $\bar{M}_{\mathrm{C}} = 0.10$. The changes in $\bar{M}_{\mathrm{C}}$ have a greater effect on deflections than changes in $\bar{M}_{\mathrm{FF}}$. There is only a relatively minor variation of energy dissipation with $\bar{M}_{\mathrm{C}}$ and $\bar{M}_{\mathrm{FF}}$.

the stress wave passes through the core. The pressure transmitted through the structure is much lower, at only 10 MPa during core crushing and reaching 40 MPa upon the completion of core crush. This value is 50% of what is seen for the structure with $\bar{M}_{\mathrm{C}} > 0.36$ and 90% of that for $\bar{M}_{\mathrm{C}} = 0.20$. On the other hand, cavitation is negligible for $\bar{M}_{\mathrm{C}} = 0.10$. Figure 11(b) shows the transmitted impulse as a function of normalized core mass $\bar{M}_{\mathrm{C}}$ and incident impulse $\bar{I}$. The relationship between transmitted impulse ($\bar{I}_{T,\mathrm{WB}}$), and incident impulse ($\bar{I}$) and normalized core mass ($\bar{M}_{\mathrm{C}}$) can be quantified by

$$\bar{I}_{T,\mathrm{WB}}/\bar{I} = 1.36 \cdot (\bar{M}_{\mathrm{C}})^{0.33}. \tag{21}$$

4.7. ***Optimal core mass.*** The previous section dealt with the role of load intensity and core mass on the dynamic response of the structures. The structure-property relations developed indicate that optimal core mass lies between 4% and 20% of the total sandwich structure mass. To further refine the analysis, a set of simulations is carried out by varying the core and front face masses while the total areal mass is held constant. Specifically, the core mass is varied from 4% to 68% of the total mass, while the front face mass is varied from 4% to 30% of the total mass. In each case, the back face mass is given by (1).

Figure 12(a) shows the normalized deflection as a function of $\bar{M}_{\mathrm{C}}$ and $\bar{M}_{\mathrm{FF}}$ for $\bar{I} = 0.5$. The results indicate that $\bar{M}_{\mathrm{C}}$ has a higher influence on deflection than $\bar{M}_{\mathrm{FF}}$ and confirm that heavy cores are detrimental to blast resistance. As the front face mass increases, the momentum transferred to the core increases, causing higher core compression and overall deflection. The highest deflection is observed for structures with maximum core and front face masses ($\bar{M}_{\mathrm{C}} = 0.68$ and $\bar{M}_{\mathrm{FF}} = 0.3$). Although core wall buckling is an essential deformation mechanism for improved blast resistance, extremely thin core walls ($\bar{M}_{\mathrm{C}} = 0.04$) can be detrimental to blast resistance, indicating that there exists a lower limit for core mass fraction. It can be concluded that the upper limit of core mass fraction is 20% while the lower limit of core mass fraction is 4% of total structural mass. Results show that structures with $\bar{M}_{\mathrm{C}} = 0.20$ undergo the least deflections due to the fact that the thickness of the core webs is sufficiently low to enable buckling and load spreading and sufficiently high to prevent complete core collapse.

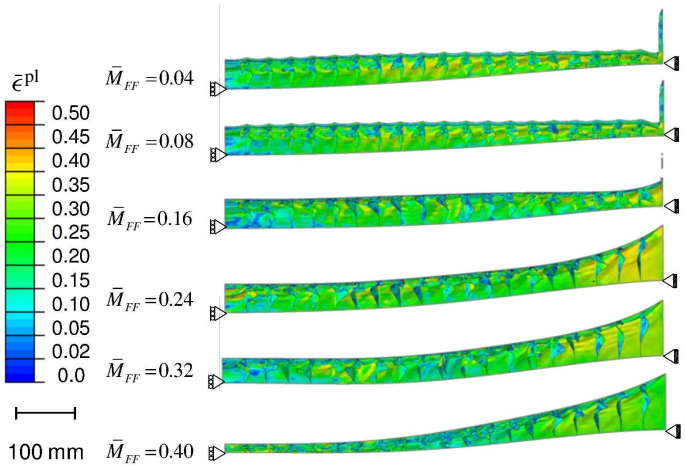

Figure 13. Distributions of equivalent plastic strain for *air-backed* structures with varying $\overline{M}_{\mathrm{FF}}$ and $\overline{M}_{\mathrm{C}} = 0.20$ subjected to an impulse of $\bar{I} = 0.2$. As $\overline{M}_{\mathrm{FF}}$ increases, the susceptibility to rupture decreases. However, heavy front faces allow lead to more severe core compression and higher deflections.

Figure 12(b) shows plastic dissipation as a function of $\overline{M}_{\mathrm{C}}$ and $\overline{M}_{\mathrm{FF}}$ for the highest impulsive load intensity ($\bar{I} = 0.5$). There are relatively minor variations in energy dissipation over the entire tested range of core and front face masses. The general trend observed in core optimization is also evident in this analysis, i.e., structures with heavy cores experience large-scale rupture and bending and show lower energy dissipation than light cores. The front face mass has a significant influence on both deflection and energy dissipation.

4.8. ***Optimization of front-face mass.*** Evaluations of the response of sandwich structures with different core strengths reveal that structures with $\overline{M}_{\mathrm{C}} \leq 0.20$ provide the best blast mitigation for the conditions analyzed. Specifically, results show that $\overline{M}_{\mathrm{C}} = 0.20$ provides high blast resistance. Furthermore, the results indicate that the front and back faces influence the deflection and energy dissipation in the entire structure. To quantify this influence, the front-face and back-face thicknesses are varied as shown in Table 2 while the core mass is maintained at $\overline{M}_{\mathrm{C}} = 0.20$. Thus, the core constitutes 20% of the total mass and core-wall buckling is the preferred deformation mechanism. The front-face mass ($\overline{M}_{\mathrm{FF}}$) is varied from 0.04 to 0.40 and the back-face mass ($\overline{M}_{\mathrm{BF}}$) is varied from 0.76 to 0.40, as shown in Table 2.

Figure 13 shows the contour plots of equivalent plastic strain at 1000 μs in air-backed structures with varying $\overline{M}_{\mathrm{FF}}$ subjected to $\bar{I} = 0.2$. Since the core mass is only 10% of the total mass, the response of the core is primarily in the form of core wall buckling. For structures with $\overline{M}_{\mathrm{FF}} = 0.04$ and $\overline{M}_{\mathrm{FF}} = 0.08$, the front face is very light and ruptures due to shear stress concentrations near the supports, followed by core-wall buckling and core compression. For structures with $\overline{M}_{\mathrm{FF}} = 0.16$, the front face ruptures due to tensile necking near the supports, followed by core wall buckling and core compression. For structures with $\overline{M}_{\mathrm{FF}} = 0.24$, the front face has sufficient strength to avoid shear or tensile failure. However, since the front face is heavier, the overall deflection is higher than those for structures with $\overline{M}_{\mathrm{FF}} < 0.24$. As $\overline{M}_{\mathrm{FF}}$ increases from 0.24 to 0.40, the front face becomes less susceptible to tensile necking and

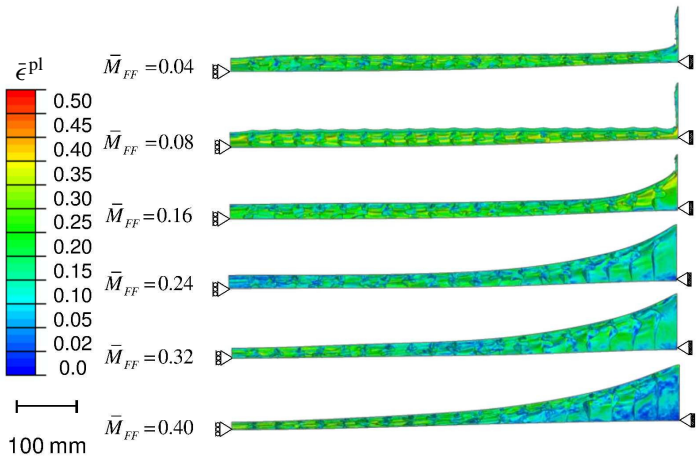

Figure 14. Distributions of equivalent plastic strain for *water-backed* structures with varying $\overline{M}_{\mathrm{FF}}$ and $\overline{M}_{\mathrm{C}} = 0.20$ subjected to an impulse of $\bar{I} = 0.2$. Heavy front faces cause progressively higher core compression as the overall deflection remains constant due to the downstream water.

rupture. However, as the front-face mass increases, more severe core compression and higher overall deflection are observed. For impulses up to $\bar{I} = 0.3$, air-backed structures with $\overline{M}_{\mathrm{FF}} \sim 0.25$, $\overline{M}_{\mathrm{C}} \sim 0.20$ and $\overline{M}_{\mathrm{BF}} \sim 0.65$ show superior blast mitigation capability. Although configurations with $\overline{M}_{\mathrm{FF}} < 0.24$ experience front-face rupture, none experience complete failure. This reinforces the fact that dynamic response is highly influenced by core mass and it is relatively less sensitive to front face mass.

Figure 14 shows the contour plots of equivalent plastic strain at 1000 μs in water-backed sandwich structures with varying $\overline{M}_{\mathrm{FF}}$ subjected to $\bar{I} = 0.2$. The failure mode for structures with $\overline{M}_{\mathrm{FF}} = 0.04, 0.08$ and 0.16 is front-face rupture near the supports followed by rapid core compression. Since the back face is constrained by back-side water, core compressive strains are much higher than those in air-backed structures. To prevent complete core collapse in the water-backed cases, it is necessary to keep $\overline{M}_{\mathrm{FF}}$ above a minimum value ($\overline{M}_{\mathrm{FF}} = 0.24$). For impulses up to $\bar{I} = 0.3$, structures with $\overline{M}_{\mathrm{FF}} \sim 0.25$, $\overline{M}_{\mathrm{C}} \sim 0.10$ and $\overline{M}_{\mathrm{BF}} \sim 0.65$ perform the best.

Figure 15 shows the normalized deflection Δ/L as a function of normalized front-face mass $\overline{M}_{\mathrm{FF}}$ and normalized impulse magnitude $\bar{I}$ in air-backed and water-backed structures. As $\overline{M}_{\mathrm{FF}}$ increases from 0.04 to 0.40, the deflection in air-backed structures increases. Structures with $\overline{M}_{\mathrm{FF}} = 0.04$ experience the smallest deflection, while those with $\overline{M}_{\mathrm{FF}} = 0.24$ and 0.40 experience deflections two and four times those for structures with $\overline{M}_{\mathrm{FF}} = 0.04$, respectively. For water-backed structures, as $\overline{M}_{\mathrm{FF}}$ increases, the overall deflection remains essentially constant due to the presence of downstream water. However, contour plots in Figures 15 and 16 show that structures with $\overline{M}_{\mathrm{FF}} < 0.24$ are susceptible to front-face rupture. Consequently, the lowest acceptable value of $\overline{M}_{\mathrm{FF}}$ is 0.24 for both air-backed and water-backed structures. The relationship between deflection $(\Delta/L)_{\mathrm{WB}}$, incident impulse $\bar{I}$ and normalized core mass $\overline{M}_{\mathrm{C}}$ in air-backed structures can be stated as

$$(\Delta/L)_{\mathrm{AB}} = 0.23 \cdot (\overline{M}_{\mathrm{FF}})^{0.27} \cdot \bar{I}^{0.62}, \tag{22}$$

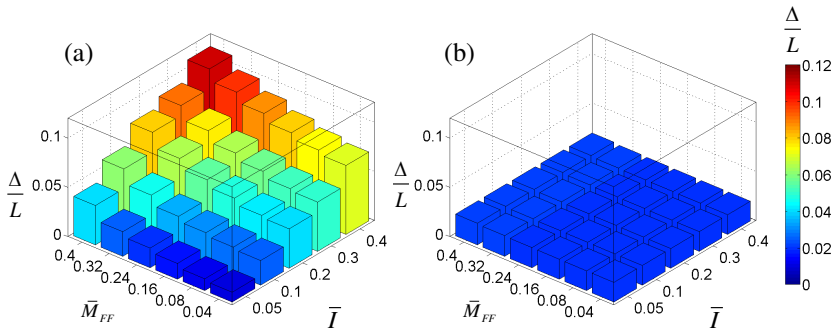

Figure 15. Deflection in (a) air-backed and (b) water-backed structures as functions of incident impulse $\bar{I}$ and normalized front-face mass $\overline{M}_{\mathrm{FF}}$ ($\overline{M}_{\mathrm{C}} = 0.20$).

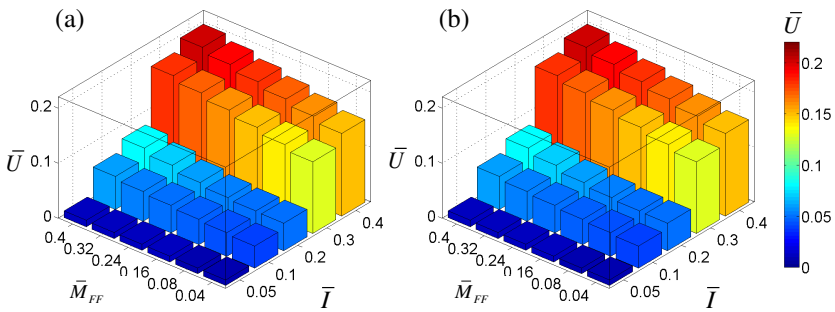

Figure 16. Energy dissipated due to plastic deformation in (a) air-backed and (b) water-backed structures as functions of incident impulse $\bar{I}$ and normalized front-face mass $\overline{M}_{\mathrm{FF}}$ ($\overline{M}_{\mathrm{C}} = 0.20$).

while that for water-backed structures can be stated as

$$(\Delta/L)_{\mathrm{WB}} = 0.02 \cdot (\overline{M}_{\mathrm{FF}})^{0.03} \cdot \bar{I}. \tag{23}$$

Figure 16 show normalized plastic dissipation $\bar{U}$ as a function of normalized front-face mass $\overline{M}_{\mathrm{FF}}$ and impulse magnitude $\bar{I}$ in air-backed and water-backed sandwich structures. For thin front faces ($\overline{M}_{\mathrm{FF}} < 0.24$), the stress wave is transmitted through the front face and into the core after the onset of loading. Tensile necking near the supports leads to rupture in the front face. Consequently, for structures with $\overline{M}_{\mathrm{FF}} < 0.24$, plastic dissipation in the core exceeds that in the front face. As $\overline{M}_{\mathrm{FF}}$ increases and the front face becomes thicker, the amount of plastic deformation in the front face increases and, as a result, the front face becomes less susceptible to rupture. Hence, the contribution of the front face to total plastic dissipation increases and that of the core decreases. For $\overline{M}_{\mathrm{FF}} = 0.4$, plastic dissipation in the front face is higher than that in the core. As discussed previously, for the same incident impulse, water-backed structures (Figure 15(b)) absorb a larger fraction of incident energy than air-backed structures. This occurs primarily through higher core-compressive strains and front-face shearing. However, the front-face plastic dissipation surpasses plastic dissipation in the core only for thick front faces with $\overline{M}_{\mathrm{FF}} = 0.4$. The relationship between plastic dissipation $\bar{U}$ in both air-backed and water-backed structures, incident

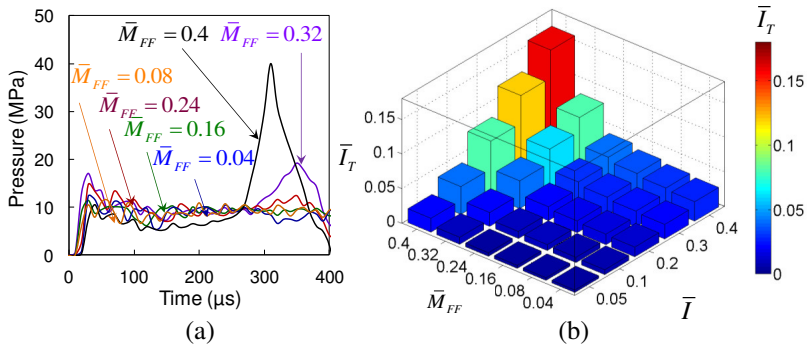

Figure 17. (a) Impulse transmission histories for $\bar{I} = 0.20$, and (b) transmitted impulse as a function of incident impulse $\bar{I}$ and normalized front-face mass $\bar{M}_{\mathrm{FF}}$ in water-backed structures ($\bar{M}_{\mathrm{C}} = 0.20$).

impulse $\bar{I}$ and normalized core mass $\bar{M}_{\mathrm{C}}$ for both air-backed and water-backed structures is

$$\bar{U} = 0.67 \cdot (\bar{M}_{\mathrm{FF}})^{0.13} \cdot \bar{I}^{1.14}. \tag{24}$$

Figure 17(a) shows the histories of transmitted pressure for water-backed structures with $\bar{M}_{\mathrm{C}} = 0.20$ and varying $\bar{M}_{\mathrm{FF}}$. The values are measured in the middle of the downstream water section. The transmitted pressure remains constant during core compression. When the core fails completely and the front face and the back face move together, a secondary pressure pulse is transmitted into the downstream water. The secondary pressure pulses for structures with $\bar{M}_{\mathrm{FF}} = 0.24$, 0.32 and 0.40 are higher in magnitude than those for structures with $\bar{M}_{\mathrm{FF}} = 0.08$, 0.16 and 0.24, due to the greater momentum acquired by the heavier front faces. As demonstrated previously, structures with $\bar{M}_{\mathrm{FF}} \leq 0.16$ undergo front-face rupture followed by core crushing and tearing near the supports. A combination of front-face mass of $\bar{M}_{\mathrm{FF}} \leq 0.24$, core mass of $\bar{M}_{\mathrm{C}} = 0.10$ and back-face mass $\bar{M}_{\mathrm{BF}} = 0.65$ provides the highest blast mitigation for air-backed as well as water-backed structures. The relationship between the transmitted impulse $\bar{I}_{T,\mathrm{WB}}$, the incident impulse $\bar{I}$ and normalized core mass $\bar{M}_{\mathrm{C}}$ (Figure 17(b)) can be given by

$$\bar{I}_{T,\mathrm{WB}}/\bar{I} = 2.82 \cdot (\bar{M}_{\mathrm{FF}})^{2.19}. \tag{25}$$

4.9. ***Structure-performance relationships.*** The preceding discussions have focused on the deformation, deflection, energy dissipation and impulse transmission in metallic sandwich structures subjected to underwater impulsive loads. In particular, the results of parametric studies have been presented in a format wherein the response variables are functions of the loading $\bar{I}$ and structural attributes ($\bar{M}_{\mathrm{C}}$, $\bar{M}_{\mathrm{FF}}$ or $\bar{M}_{\mathrm{BF}}$). Analyses show that such contact conditions play an important role in the response of sandwich structures to underwater blasts. Structural design must satisfy prescribed performance objectives through identification of proper structural attributes that fulfill the requirements. Here, deflection, impulse transmission, and energy dissipation are taken as the performance metrics. These metrics may pose competing requirements on structure attributes. In both air-backed and water-backed structures, the energy dissipated in the entire structure follows a similar trend. Deflection is a relatively less useful metric in water-backed structures due to the fact that the presence of downstream water keeps deflection small. In such cases,

Figure	Contact condition	Acceptance metric	Structure-performance relations
Figure 7(a)	Air-backed	Deflection	$(\Delta/L)_{\mathrm{AB}} = 1.58\,(\overline{M}_{\mathrm{C}})^{0.24}\,\overline{I}^{0.86}$
Figure 9(a)		Energy dissipation	$\overline{U}_{\mathrm{AB}} = 0.22\,(\overline{M}_{\mathrm{C}})^{-0.20}\,\overline{I}^{1.07}$
Figure 7(b)	Water-backed	Deflection	$(\Delta/L)_{\mathrm{WB}} = 0.43\,(\overline{M}_{\mathrm{C}})^{0.22}\,\overline{I}^{0.85}$
Figure 9(b)		Energy dissipation	$\overline{U}_{\mathrm{WB}} = 0.20\,(\overline{M}_{\mathrm{C}})^{-0.21}\,\overline{I}^{0.69}$
Figure 11(b)		Impulse transmission	$\overline{I}_{T,\mathrm{WB}}/\overline{I} = 1.36\,(\overline{M}_{\mathrm{C}})^{0.33}$

Table 4. Summary of material-structure-property relationships for core optimization.

Figure	Contact condition	Acceptance metric	Structure-performance relations
Figure 15(a)	Air-backed	Deflection	$(\Delta/L)_{\mathrm{AB}} = 0.23\,(\overline{M}_{\mathrm{FF}})^{0.27}\,\overline{I}^{0.62}$
Figure 15(b)		Energy dissipation	$\overline{U}_{\mathrm{AB}} = 0.67\,(\overline{M}_{\mathrm{FF}})^{0.13}\,\overline{I}^{1.14}$
Figure 15(c)	Water-backed	Deflection	$(\Delta/L)_{\mathrm{WB}} = 0.02\,(\overline{M}_{\mathrm{FF}})^{0.03}\,\overline{I}$
Figure 15(d)		Energy dissipation	$\overline{U}_{\mathrm{WB}} = 0.67\,(\overline{M}_{\mathrm{FF}})^{0.13}\,\overline{I}^{1.14}$
Figure 17(b)		Impulse transmission	$\overline{I}_{T,\mathrm{WB}}/\overline{I} = 2.82\,(\overline{M}_{\mathrm{FF}})^{2.19}$

Table 5. Summary of material-structure-property relationships for front-face optimization.

the transmitted impulse (measured in the back-side water section) may be a more relevant and useful quantity. The structure-performance relations are summarized in Table 4 and Table 5.

An optimal sandwich structure design needs to balance low deflection and high energy dissipation. This balance is application-specific and may not be universal. The relations developed in this study allow the identification of optimal structural designs for given combination of deflection, energy dissipation and impulse transmission requirements. For a given level of deflection or energy dissipation, the optimum value of core or face masses for a specific impulsive load can be achieved by varying the component thicknesses. The focus of this analysis is on the development of quantitative relations which can be used by structural designers. As discussed previously, core mass is the most critical structural attribute of a sandwich structure. Although (16) gives a simple relationship between core mass, impulse magnitude and deflection, it must be noted that $\overline{M}_{\mathrm{C}} = 0.04$ is the *lower* limit of core mass. The material-structure-performance relations can be used to inform structural design with the precaution that they should only be used for the material, structural parameter ranges and loading conditions considered.

5. Concluding remarks

To be resilient to impulsive loading, structures must balance rigidity, load-carrying capacity and an ability to dissipate energy. Sandwich composites, with a combination of stiff face sheets and compliant cores, can provide high shear and bending resistances, as well as an ability to absorb energy. In an effort to provide quantitative relations for structural design, we have evaluated the performance in terms of deflection and energy-dissipation of metal sandwich structures under high-intensity impulsive loading over a range of structural attributes and loading. In particular, the conditions analyzed involve impulsive loads with peak pressures up to 450 MPa and impulses up to 41 kPa·s. This range of load profiles is

indicative of the effects at different standoff distances of 100 kg of TNT detonating underwater. The present work has focused on the damage and deformation occurring in blast-loaded metallic sandwich plates in the early stages of deformation and the role of loading intensity and structural attributes on dynamic performance. The constitutive and damage models used in the analysis are capable of capturing the effects of different inelastic deformation and failure mechanisms in the face sheets and sandwich cores. The calculations have yielded the following findings.

There is a close relationship between structural parameters, loading rates and dynamic performance. The performance of metallic sandwich structures is significantly influenced by core mass and core wall thickness. For cores with $\overline{M}_{\mathrm{C}} > 0.20$, deformation is dominated by bending and core-stretching. For cores with $\overline{M}_{\mathrm{C}} \leq 0.20$, deformation is dominated by core-wall buckling and front-face stretching. Although light core structures provide significantly higher blast mitigation compared to heavy core structures on a per-unit weight basis, there exists a lower limit of core mass below which the structural benefits of light cores are lost due to core collapse. This lower limit is approximately $\overline{M}_{\mathrm{C}} = 0.10$. Below this limit, deformation is dominated by core-wall buckling and crushing and the front face strikes the back face due to core failure. A combination of core-wall buckling and load-spreading provides the highest blast mitigation. This combination is achieved when the core mass is $\sim 20\%$ of the total structural mass, as measured by $\overline{M}_{\mathrm{C}}$ and $\overline{M}_{\mathrm{FF}}$ in the analysis.

Deformation and energy dissipation are relatively less sensitive to front-face mass, as compared to core mass. However, an optimal design requires a balance between core and face sheet masses ($\overline{M}_{\mathrm{C}} = 0.20$, $\overline{M}_{\mathrm{FF}} > 0.20$). The back-face mass has negligible effect on overall blast resistance in the initial stages of deformation. However, thick back faces are significantly less susceptible to rupture and exhibit improved blast resistance. For impulses up to $\bar{I} = 0.5$, sandwich structures with $\overline{M}_{\mathrm{FF}} \sim 0.25$, $\overline{M}_{\mathrm{C}} \sim 0.20$ and $\overline{M}_{\mathrm{BF}} \sim 0.55$ provide the highest bending resistance. The results suggest that the role of support conditions is very important in designing sandwich plates resistant to underwater blasts. In particular, for heavy core structures, clamped boundary conditions lead to shear-dominated rupture which is highly dependent on support conditions.

The responses of structures under air-backed and water-backed conditions are significantly different. Deflections under water-backed conditions are $\sim 30\%$ of the deflections under air-backed conditions for $\overline{M}_{\mathrm{C}} < 0.20$ and $\sim 60\%$ for $\overline{M}_{\mathrm{C}} > 0.20$ at high impulse magnitudes. However, for both air-backed and water-backed conditions, structures with $\overline{M}_{\mathrm{C}} = 0.10$ show the lowest deflection, and, therefore, the highest bending resistance. Under the same loading conditions, the dissipation in water-backed structures is $\sim 20\%$ higher than the dissipation in air-backed structures.

The calculations have yielded quantitative structure-performance relations in terms of deflection, energy dissipation, and load transmission. These relations allow optimal or desirable structure attributes to be identified for prescribed loading conditions or performance targets. These relations can provide guidance for the design of blast-resistant metallic structures. Finally, it should be noted that the relations described in this paper are applicable only for the structural attributes and loading conditions considered.

6. Acknowledgement

The authors gratefully acknowledge support by the Office of Naval Research through grant numbers N00014-09-1-0808 and N00014-09-1-0618 (program manager: Dr. Yapa D. S. Rajapakse). Calculations

were carried out on the HPC cluster in the DPRL at Georgia Tech. Min Zhou also acknowledges beneficial interactions through the CAS/SAFEA International Partnership Program for Creative Research Teams.

References

[Battley and Allen 2012] M. Battley and T. Allen, "Servo-hydraulic system for controlled velocity water impact of marine sandwich panels", *Exp. Mech.* **52**:1 (2012), 95–106.

[Cole 1947] R. H. Cole, "Spherical shock waves from underwater explosions", *Phys. Rev.* **72**:2 (1947), 177.

[ConWep 2005] ConWep, "ConWep blast simulation software", 2005, https://pdc.usace.army.mil/software/conwep/.

[Côté et al. 2009] F. Côté, B. P. Russell, V. S. Deshpande, and N. A. Fleck, "The through-thickness compressive strength of a composite sandwich panel with a hierarchical square honeycomb sandwich core", *J. Appl. Mech.* (*ASME*) **76**:6 (2009), 061004.

[Deshpande and Fleck 2005] V. S. Deshpande and N. A. Fleck, "One-dimensional response of sandwich plates to underwater shock loading", *J. Mech. Phys. Solids* **53**:11 (2005), 2347–2383.

[Dharmasena et al. 2008] K. P. Dharmasena, H. N. G. Wadley, Z. Xue, and J. W. Hutchinson, "Mechanical response of metallic honeycomb sandwich panel structures to high-intensity dynamic loading", *Int. J. Impact Eng.* **35**:9 (2008), 1063–1074.

[Dharmasena et al. 2010] K. P. Dharmasena, D. T. Queheillalt, H. N. G. Wadley, P. Dudt, Y. Chen, D. Knight, A. G. Evans, and V. S. Deshpande, "Dynamic compression of metallic sandwich structures during planar impulsive loading in water", *Eur. J. Mech. A Solids* **29**:1 (2010), 56–67.

[Dharmasena et al. 2011] K. P. Dharmasena, H. N. G. Wadley, K. Williams, Z. Xue, and J. W. Hutchinson, "Response of metallic pyramidal lattice core sandwich panels to high intensity impulsive loading in air", *Int. J. Impact Eng.* **38**:5 (2011), 275–289.

[Espinosa et al. 2006] H. D. Espinosa, S. Lee, and N. Moldovan, "A novel fluid structure interaction experiment to investigate deformation of structural elements subjected to impulsive loading", *Exp. Mech.* **46**:6 (2006), 805–824.

[Hibbit et al. 2009] D. Hibbit, B. Karlsson, and P. Sorensen, *Abaqus/Explicit user's manual, version 6.9*, ABAQUS, Cambridge, 2009, http://abaqusdoc.ucalgary.ca/v6.9/.

[Hutchinson and Xue 2005] J. W. Hutchinson and Z. Xue, "Metal sandwich plates optimized for pressure impulses", *Int. J. Mech. Sci.* **47**:4–5 (2005), 545–569.

[Johnson and Cook 1985] G. R. Johnson and W. H. Cook, "Fracture characteristics of three metals subjected to various strains, strain rates, temperatures and pressures", *Eng. Fract. Mech.* **21**:1 (1985), 31–48.

[Kambouchev et al. 2007] N. Kambouchev, L. Noels, and R. Radovitzky, "Numerical simulation of the fluid–structure interaction between air blast waves and free-standing plates", *Comput. Struct.* **85**:11–14 (2007), 923–931.

[Latourte et al. 2012] F. Latourte, X. Wei, Z. D. Feinberg, A. de Vaucorbeil, P. Tran, G. B. Olson, and H. D. Espinosa, "Design and identification of high performance steel alloys for structures subjected to underwater impulsive loading", *Int. J. Solids Struct.* **49**:13 (2012), 1573–1587.

[Liang et al. 2005] Y. Liang, A. V. Spuskanyuk, S. E. Flores, D. R. Hayhurst, J. W. Hutchinson, R. M. McMeeking, and A. G. Evans, "The response of metallic sandwich panels to water blast", *J. Appl. Mech.* (*ASME*) **74**:1 (2005), 81–99.

[McShane et al. 2006] G. J. McShane, V. S. Deshpande, and N. A. Fleck, "The underwater blast resistance of metallic sandwich beams with prismatic lattice cores", *J. Appl. Mech.* (*ASME*) **74**:2 (2006), 352–364.

[McShane et al. 2008] G. J. McShane, C. Stewart, M. T. Aronson, H. N. G. Wadley, N. A. Fleck, and V. S. Deshpande, "Dynamic rupture of polymer–metal bilayer plates", *Int. J. Solids Struct.* **45**:16 (2008), 4407–4426.

[Mori et al. 2007] L. F. Mori, S. Lee, Z. Y. Xue, A. Vaziri, D. T. Queheillalt, K. P. Dharmasena, H. N. G. Wadley, J. W. Hutchinson, and H. D. Espinosa, "Deformation and fracture modes of sandwich structures subjected to underwater impulsive loads", *J. Mech. Mater. Struct.* **2**:10 (2007), 1981–2006.

[Nahshon et al. 2007] K. Nahshon, M. G. Pontin, A. G. Evans, J. W. Hutchinson, and F. W. Zok, "Dynamic shear rupture of steel plates", *J. Mech. Mater. Struct.* **2**:10 (2007), 2049–2066.

[Radford et al. 2006] D. D. Radford, G. J. McShane, V. S. Deshpande, and N. A. Fleck, "Dynamic compressive response of stainless-steel square honeycombs", *J. Appl. Mech.* (*ASME*) **74**:4 (2006), 658–667.

[Rathbun et al. 2006] H. J. Rathbun, D. D. Radford, Z. Xue, M. Y. He, J. Yang, V. Deshpande, N. A. Fleck, J. W. Hutchinson, F. W. Zok, and A. G. Evans, "Performance of metallic honeycomb-core sandwich beams under shock loading", *Int. J. Solids Struct.* **43**:6 (2006), 1746–1763.

[Spuskanyuk and McMeeking 2007] A. V. Spuskanyuk and R. M. McMeeking, "Sandwich panels for blast protection in water: Simulations", *Int. J. Mater. Res.* **98**:12 (2007), 1250–1255.

[Taylor 1963] G. I. Taylor, *Scientific papers, III: Aerodynamics and the mechanics of projectiles and explosions*, edited by G. K. Batchelor, Cambridge University Press, 1963.

[Vaziri and Xue 2007] A. Vaziri and Z. Xue, "Mechanical behavior and constitutive modeling of metal cores", *J. Mech. Mater. Struct.* **2**:9 (2007), 1743–1760.

[Vaziri et al. 2007] A. Vaziri, Z. Xue, and J. W. Hutchinson, "Performance and failure of metal sandwich plates subjected to shock loading", *J. Mech. Mater. Struct.* **2**:10 (2007), 1947–1963.

[Wadley et al. 2013] H. N. G. Wadley, T. Børvik, L. Olovsson, J. J. Wetzel, K. P. Dharmasena, O. S. Hopperstad, V. S. Deshpande, and J. W. Hutchinson, "Deformation and fracture of impulsively loaded sandwich panels", *J. Mech. Phys. Solids* **61**:2 (2013), 674–699.

[Wei et al. 2008] Z. Wei, V. S. Deshpande, A. G. Evans, K. P. Dharmasena, D. T. Queheillalt, H. N. G. Wadley, Y. V. Murty, R. K. Elzey, P. Dudt, Y. Chen, D. Knight, and K. Kiddy, "The resistance of metallic plates to localized impulse", *J. Mech. Phys. Solids* **56**:5 (2008), 2074–2091.

[Wicks and Hutchinson 2001] N. Wicks and J. W. Hutchinson, "Optimal truss plates", *Int. J. Solids Struct.* **38**:30–31 (2001), 5165–5183.

[Xue and Hutchinson 2004a] Z. Xue and J. W. Hutchinson, "A comparative study of impulse-resistant metal sandwich plates", *Int. J. Impact Eng.* **30**:10 (2004), 1283–1305.

[Xue and Hutchinson 2004b] Z. Xue and J. W. Hutchinson, "Constitutive model for quasi-static deformation of metallic sandwich cores", *Int. J. Numer. Methods Eng.* **61**:13 (2004), 2205–2238.

[Zok et al. 2003] F. W. Zok, H. J. Rathbun, Z. Wei, and A. G. Evans, "Design of metallic textile core sandwich panels", *Int. J. Solids Struct.* **40**:21 (2003), 5707–5722.

[Zok et al. 2005] F. W. Zok, H. Rathbun, M. He, E. Ferri, C. Mercer, R. M. McMeeking, and A. G. Evans, "Structural performance of metallic sandwich panels with square honeycomb cores", *Philos. Mag.* **85**:26–27 (2005), 3207–3234.

Received 20 Mar 2014. Revised 16 Oct 2014. Accepted 19 Oct 2014.

SIDDHARTH AVACHAT: sidavachat@gmail.com
The George W. Woodruff School of Mechanical Engineering, The School of Materials Science and Engineering, Georgia Institute of Technology, Atlanta, GA 30332-0405, United States

MIN ZHOU: min.zhou@gatech.edu
The George W. Woodruff School of Mechanical Engineering, The School of Materials Science and Engineering, Georgia Institute of Technology, Atlanta, GA 30332-0405, United States

JOURNAL OF MECHANICS OF MATERIALS AND STRUCTURES

msp.org/jomms

Founded by Charles R. Steele and Marie-Louise Steele

Cover photo: Ev Shafrir

See msp.org/jomms for submission guidelines.

JoMMS (ISSN 1559-3959) at Mathematical Sciences Publishers, 798 Evans Hall #6840, c/o University of California, Berkeley, CA 94720-3840, is published in 10 issues a year. The subscription price for 2015 is US $565/year for the electronic version, and $725/year (+$60, if shipping outside the US) for print and electronic. Subscriptions, requests for back issues, and changes of address should be sent to MSP.

JoMMS peer-review and production is managed by EditFLOW® from Mathematical Sciences Publishers.

PUBLISHED BY

mathematical sciences publishers

nonprofit scientific publishing

http://msp.org/

Journal of Mechanics of Materials and Structures

Volume 10, No. 1 January 2015

Flexural behavior of functionally graded slender beams with complex cross-section
GHOLAMALI SHARIFISHOURABI, AMRAN AYOB, SOHEIL GOHARI, MOHD YAZID BIN YAHYA, SHOKROLLAH SHARIFI and ZORA VRCELJ 1

Response of submerged metallic sandwich structures to underwater impulsive loads
SIDDHARTH AVACHAT and MIN ZHOU 17

Thermal and magnetic effects on the vibration of a cracked nanobeam embedded in an elastic medium
DANILO KARLIČIĆ, DRAGAN JOVANOVIĆ, PREDRAG KOZIĆ and MILAN CAJIĆ 43

Contours for planar cracks growing in three dimensions
LOUIS MILTON BROCK 63

Mechanical degradation of natural fiber reinforced composite materials under constrained swelling
YIHUI PAN and ZHENG ZHONG 79

On the occurrence of lumped forces at corners in classical plate theories: a physically based interpretation
LAURA GALUPPI and GIANNI ROYER-CARFAGNI 93